Advanced Vehicle State Estimation: A Tutorial and Comparative Study

Jay A. Farrell   Paul F. Roysdon [*]

[*] *University of California, Riverside, CA 92521 USA*
(e-mail: farrell@ece.ucr.edu, proysdon@ece.ucr.edu).

Abstract: Autonomous vehicles require high bandwidth, high sample rate, precision vehicle and world relative state estimation, especially those such as automobiles that involve human safety with a mixed set of vehicles operating in a complex environment containing humans. An additional requirement is high reliability. Such systems will ultimately involve a multiplicity of sensor modalities. Sensor fusion is critical to achieving these application requirements. Several of the sensors (e.g., vision, radar, Lidar, ultrasound, Global Navigation Satellite Systems (GNSS)) have various spurious measurement types. Standard Extended Kalman Filter (EKF) approaches are not sufficiently reliable at removing the effects of such spurious measurements. The EKF approach must decide at the time each measurement arrives whether it is valid. If so, the measurement is used and discarded; otherwise it is not used and discarded. When that decision is wrong, either measurement information is lost or the state and covariance estimates are corrupted. Either situation can result in divergence of the EKF. An alternative is to maintain all recent measurement data within a moving time-horizon. This window of data can be processed within a Bayesian framework to extract the optimal state trajectory estimate over the time-horizon, under various fault scenario assumptions. Because the time window of data is maintained it is straightforward to change the assumptions as to which data are valid and reprocess the data. Therefore, in prior articles, this approach was referred to as a Contemplative Real-Time (CRT) estimator. It is closely related to Moving Horizon Estimation (MHE) and Simultaneous Localization and Mapping (SLAM). This paper has tutorial content explaining the interrelationships between the EKF, Iterated Extended Kalman Filter (IEKF), and CRT within the Bayesian framework; discussion of the fault detection procedures, and comparative experimental results.

Keywords: Moving Horizon Estimation (MHE), Simultaneous Localization and Mapping (SLAM), Extended Kalman Filter (EKF)

1. INTRODUCTION

Autonomous vehicles are rapidly transitioning toward commercialization. Aircraft and quadcopters are already available. Air and undersea vehicles are used in both military and commercial applications. Land vehicles are already used in mining, farming, warehouse, and harbor applications. However, certain life-safety critical applications, e.g. roadway vehicles, are still in the research stage.

One critical challenge is reliable, high-rate, high bandwidth estimation of the vehicle state at submeter, ideally decimeter, accuracy. This is the main topic of this article. The article will assume an aided inertial navigation approach (Farrell (2008)). Inertial navigation system (INS) approaches integrate specific force and angular rate measurements from an inertial measurement unit (IMU) through the kinematic model of an instrument platform. This approach continuously provides a full state estimate (e.g., position, velocity, attitude) plus acceleration and angular rate, with the system bandwidth and update rate determined by the characteristics of the IMU and implementation computer. Bandwidth and update rates in the hundreds to thousands of Hertz are standard. Due to

these factors, since the 1960's, aided inertial approaches typically implemented using an extended Kalman filter (Brown and Hwang (1983); Jazwinski (1970); Kalman (1960); Kalman and Bucy (1961); Maybeck (1979)), have been the standard approach for almost all military, commercial, and space applications involving safety of human life.

A few factors distinguish highway vehicle applications from those applications cited above. One aspect is the accuracy requirements. Typical lane widths in the US are approximately $3.6m$ and a vehicle width can exceed $2m$; therefore, to ensure worst-case control errors less than a meter, lane relative position estimation accuracy better than $0.1m$ is desirable. Another aspect for such commercial applications is the requirement of low cost. Yet another aspect is the challenging operational environment. Highway vehicles will be expected to operate under foliage, in dense urban canyons, feature devoid deserts or snow covered terrain, and open sky rural environments.

Various different aspects of accuracy are important. The class of sensors referred to herein as *aiding* sensors (e.g., GNSS, vision, Lidar, Radar) provide information for estimation of pose (position and/or attitude) at the sensor

sample rate, with predictable uniform accuracy, when the sensor data and processing is valid. When the sensor data is unavailable or invalid, the pose estimate is not available. Data availability and validity is affected by numerous factors external to the sensor. When aiding sensor data is available, differentiation is necessary to estimate velocity, acceleration, and angular rate. Differentiation amplifies high-frequency noise. Even if the aiding sensor sample rate is increased, the bandwidth of the estimate may be limited by factors within the sensor, such that the bandwidth of the state estimate does not increase with the sample rate. Inertial navigation has the opposite characteristics. The IMU data availability is completely independent of external factors. The IMU data provides the full state estimate through an integrative process, such that the error covariance of the state estimation process grows continuously, but in a smooth and very predictable fashion. The motivation for combining these sensors together in the state estimation process is to achieve the best aspects of both types of sensors.

In aided inertial navigation approaches, the INS integrates the IMU data continuously, always providing the full state estimate (plus acceleration and angular rate) with bandwidth and frequency as determined by the IMU. As the aiding sensor data becomes available, it is incorporated through a sensor fusion process to correct the INS state (Farrell et al. (2000)). This combined approach achieves the bandwidth, sample rate, and continuity specifications of the INS approach together with the predictable and uniform accuracy of the aiding sensors. The entire process only involves integration, not differentiation.

Also critical is the reliability of the state estimation process to erroneous sensor data. This topic is a main focus of this article. This article is not concerned with *failures* of the sensors. It is concerned with preventing invalid or incorrect measurements from significantly affecting the vehicle state estimate in real-time.

2. BACKGROUND AND NOTATION

This section introduces notation and INS background.

2.1 Aided Inertial Navigation

Let $\boldsymbol{x} \in \mathbb{R}^n$ denote the rover state vector. The kinematic equations for the rover state are

$$\dot{\boldsymbol{x}}(t) = \boldsymbol{f}(\boldsymbol{x}(t), \boldsymbol{u}(t)), \tag{1}$$

where $\boldsymbol{u} \in \mathbb{R}^6$ is the specific force and angular rate vector and $\boldsymbol{f} : \mathbb{R}^n \times \mathbb{R}^6 \mapsto \mathbb{R}^n$. Typical values of n exceed 15. The function $\boldsymbol{f}$ is the kinematic model which is accurately known (e.g., see eqns. (11.31-11.33) in Farrell (2008) or Farrell et al. (2000)).

Given a distribution for the state initial condition $\boldsymbol{x}(0) \sim N(\hat{\boldsymbol{x}}(0), \boldsymbol{P}(0))$ and measurements $\tilde{\boldsymbol{u}}$ of $\boldsymbol{u}$, an Inertial Navigation System (INS) propagates an estimate of the vehicle state between aiding measurement times as a solution of

$$\dot{\hat{\boldsymbol{x}}}(t) = \boldsymbol{f}(\hat{\boldsymbol{x}}(t), \tilde{\boldsymbol{u}}(t)), \tag{2}$$

where $\hat{\boldsymbol{x}}(t)$ denotes the estimate of $\boldsymbol{x}(t)$. The INS numerically solves eqn. (2) in discrete-time at the (high-rate) IMU sample times:

$$\hat{\boldsymbol{x}}(\tau_{i+1}) = \boldsymbol{\phi}(\hat{\boldsymbol{x}}(\tau_i), \hat{\boldsymbol{u}}(\tau_i))$$
$$= \hat{\boldsymbol{x}}(\tau_i) + \int_{\tau_i}^{\tau_{i+1}} \boldsymbol{f}(\hat{\boldsymbol{x}}(\tau), \hat{\boldsymbol{u}}(\tau)) d\tau \tag{3}$$

where τ_i represents the i-th IMU sample time. The result of the numeric integration [1] of eqn. (3) is the INS state estimate for $\hat{\boldsymbol{x}}(\tau_{i+1})$ given $\hat{\boldsymbol{x}}(\tau_i)$ and $\hat{\boldsymbol{u}}(\tau_i)$. The numeric integration repeats at each IMU sample time to maintain the real-time state estimate between the times of aiding measurements. The aiding measurement times can be unequally spaced in time without causing any complications.

Let $\tilde{\mathbf{U}}_k = \{\tilde{\boldsymbol{u}}(\tau_i), \ \tau_i \in [t_k, t_{k+1}]\}$, where t_k represents the time of the k-th aiding measurement. Eqn. (3) can be used recursively to compute $\hat{\boldsymbol{x}}_{k+1} = \hat{\boldsymbol{x}}(t_{k+1})$ from $\hat{\boldsymbol{x}}_k = \hat{\boldsymbol{x}}(t_k)$ and $\tilde{\mathbf{U}}_k$. Denote this as

$$\hat{\boldsymbol{x}}_{k+1} = \boldsymbol{\phi}(\hat{\boldsymbol{x}}_k, \tilde{\mathbf{U}}_k)). \tag{4}$$

Due to initial condition errors, system calibration errors, and measurement noise, the state estimation error $\delta\boldsymbol{x}(t) = \boldsymbol{x}(t) - \hat{\boldsymbol{x}}(t)$ develops over time. Over any time interval $[t_k, t_{k+1}]$, the linearized error growth model is

$$\delta\hat{\boldsymbol{x}}_{k+1} = \boldsymbol{\Phi}_k \delta\hat{\boldsymbol{x}}_k + \boldsymbol{\omega}_k \tag{5}$$

where $\boldsymbol{\omega}_k \sim N(\mathbf{0}, \mathbf{Q}_k)$ and $\boldsymbol{\Phi}_k = \frac{\partial \boldsymbol{\phi}(\boldsymbol{x})}{\partial \boldsymbol{x}}\big|_{(\hat{\boldsymbol{x}}_k, \tilde{\mathbf{U}}_k)}$. The INS provides both $\mathbf{Q}_k$ and $\boldsymbol{\Phi}_k$, see §7.2.5.2 in (Farrell (2008)).

2.2 Aiding Sensor Model

The aiding sensor measurements are modeled as

$$\tilde{\boldsymbol{z}}_k = \boldsymbol{h}(\boldsymbol{x}_k) + \boldsymbol{\eta}_k + \boldsymbol{e}_k \tag{6}$$

where $\boldsymbol{h} : \mathbb{R}^n \mapsto \mathbb{R}^m$ is a known function, $\boldsymbol{\eta}_k \sim N(\mathbf{0}, \boldsymbol{R}_k)$ represents a normally distributed measurement noise vector, and $\boldsymbol{e}_k$ represents other measurement inaccuracies. At most measurement time instants t_k, $\boldsymbol{e}_k = \mathbf{0}$ and the sensor data at that time is said to be valid. At those time instants when $\boldsymbol{e}_k \neq \mathbf{0}$ and is large relative to the covariance $\boldsymbol{R}_k$, the aiding sensor data $\tilde{\boldsymbol{z}}_k$ is considered to be an *outlier*.

The linearized measurement model for the residual measurement $\delta\boldsymbol{z}_k = \tilde{\boldsymbol{z}}_k - \boldsymbol{h}(\hat{\boldsymbol{x}}_k)$ is

$$\delta\boldsymbol{z}_k = \boldsymbol{H}_k \delta\boldsymbol{x}_k + \boldsymbol{\eta}_k + \boldsymbol{e}_k \tag{7}$$

where $\boldsymbol{H}_k = \frac{\partial \boldsymbol{h}}{\partial \boldsymbol{x}}\big|_{\hat{\boldsymbol{x}}_k}$.

In the theoretical portions of this article, to simplify the notation and discussion, we assumed that aiding measurements are aligned with IMU times and consider $m_k = m$ to be constant with $t_k = kT$ where T is the aiding sensor sample rate, and $(\tau_{i+1} - \tau_i) \ll T$. The experimental results later in the paper accommodate the typical realities that sensor measurement times are not aligned and that m_k is not constant.

3. PROBLEM STATEMENTS

For a known linear system with white normally distributed process and measurement noise vectors with known covariance, the Kalman filter (KF) is the optimal (linear or nonlinear) estimator. The KF can be derived from a variety

---

[1] The error state that is estimated in the sensor fusion process will include various sensor calibration parameters (e.g., biases or scale factors). The symbol $\hat{\boldsymbol{u}}$ in eqn. (3) represents the IMU measurements after being corrected using the estimated calibration parameters.

of perspectives (Maybeck (1979); Jazwinski (1970)), e.g.: Maximum a Posteriori (MAP), or Minimum Mean Squared Error. When the time propagation or measurement models are nonlinear, a variety of methods are available to solve the sensor fusion problem. The problem statement for those of interest herein are defined in this section. We present each within the Bayesian MAP framework.

3.1 Extended Kalman Filter (EKF)

Given the *a posteriori* state estimate $\hat{\boldsymbol{x}}_{k-1}$ and its error covariance matrix $\boldsymbol{P}_{k-1}$ from time t_{k-1}, as the IMU data arrives the INS iterates eqn. (3) until it has computed the *a priori* state estimate $\hat{\boldsymbol{x}}_k^- = \boldsymbol{\phi}\big(\hat{\boldsymbol{x}}_{k-1}, \hat{\mathbf{U}}_{k-1}\big)$, from which it computes the *a priori* predicted measurement $\hat{\boldsymbol{z}}_k = \boldsymbol{h}(\boldsymbol{x}_k^-)$. The EKF uses the error state model eqn. (5) to propagate the error covariance matrix

$$\boldsymbol{P}_k^- = \boldsymbol{\Phi}_{k-1}\boldsymbol{P}_{k-1}\boldsymbol{\Phi}_{k-1}^\top + \mathbf{Q}_{k-1}. \tag{8}$$

Considering $\boldsymbol{x}_k \sim N(\hat{\boldsymbol{x}}_k^-, \boldsymbol{P}_k^-)$ and $\boldsymbol{z}_k \sim N(\hat{\boldsymbol{z}}_k, \boldsymbol{R}_k)$, the *a priori* distribution for $\delta\boldsymbol{x}_k$ is $N(\boldsymbol{0}, \boldsymbol{P}_k^-)$. Assuming the absence of outliers (i.e., $\boldsymbol{e}_k = \boldsymbol{0}$), the *a priori* distribution for the measurement residual is $\delta\boldsymbol{z}_k \sim N(\boldsymbol{0}, \boldsymbol{S}_k)$, where $\delta\boldsymbol{z}_k$ is modeled by eqn. (7) and $\boldsymbol{S}_k = \boldsymbol{H}_k\boldsymbol{P}_k\boldsymbol{H}_k^\top + \boldsymbol{R}_k$. Given these facts, the EKF error state estimate can be formulated as

$$\delta\hat{\boldsymbol{x}}_k = \arg\max_{\delta\boldsymbol{x}_k} \Big(p_{\boldsymbol{\eta}_k}\big(\delta\boldsymbol{z}_k | \delta\boldsymbol{x}_k\big)p_{\delta\boldsymbol{x}_k}\big(\delta\boldsymbol{x}_k\big)\Big), \tag{9}$$

where the measurement residual $\delta\boldsymbol{z}_k$ is known. Dropping the subscript k's, the log-likelihood function is

$$(\delta\boldsymbol{z} - \boldsymbol{H}\delta\boldsymbol{x})^\top \boldsymbol{R}^{-1} (\delta\boldsymbol{z} - \boldsymbol{H}\delta\boldsymbol{x}) + \delta\boldsymbol{x}^\top (\boldsymbol{P}^-)^{-1}\delta\boldsymbol{x}$$

which is minimized by the $\delta\boldsymbol{x}$ that solves

$$\big(\boldsymbol{H}^\top\boldsymbol{R}^{-1}\boldsymbol{H} + (\boldsymbol{P}^-)^{-1}\big)\delta\boldsymbol{x} = \boldsymbol{H}^\top\boldsymbol{R}^{-1}\delta\boldsymbol{z}, \tag{10}$$

which for a linear system is equivalent to the standard KF (see §5.3.3-5.3.4 in Farrell (2008)).

Given this $\delta\hat{\boldsymbol{x}}_k$, it is used to correct the *a priori* state $\hat{\boldsymbol{x}}_k^-$. We will write the correction as $\hat{\boldsymbol{x}}_k = \hat{\boldsymbol{x}}_k^- + \delta\hat{\boldsymbol{x}}_k$; however, the actual operations are more complicated as the attitude corrections are multiplicative, not additive. The *a posteriori* error covariance matrix is $\boldsymbol{P}_k = \big(\boldsymbol{H}^\top\boldsymbol{R}^{-1}\boldsymbol{H} + (\boldsymbol{P}^-)^{-1}\big)^{-1}$, where $\boldsymbol{H}^\top\boldsymbol{R}^{-1}\boldsymbol{H} + (\boldsymbol{P}^-)^{-1}$ is the corresponding information matrix.

Remark 1. Standard EKF assumptions are that:

- initially all states are uncertain (i.e., $\boldsymbol{P}_0$ is positive definite); and,
- the state is controllable from the driving noise $\boldsymbol{\omega}_k$ (i.e., $\boldsymbol{Q}_k$ is positive definite).

These assumptions ensure that $\boldsymbol{P}_k$ and $\boldsymbol{P}_k^-$ are nonsingular; therefore, eqn. (10) has a unique solution. $\triangle$

Remark 2. In the EKF, during the measurement update, the prior $\hat{\boldsymbol{x}}_k^-$ and its distribution are unchangeable and assumed to be without error. The measurement residuals can be analyzed relative to their predicted covariance to detect and remove outliers; however, if correct measurements are removed, then measurement information is lost. More critically, if outliers are missed, they corrupt $\hat{\boldsymbol{x}}_k$ such that $N(\hat{\boldsymbol{x}}_k, \boldsymbol{P}_k)$ is not a valid model for the state estimate

$\hat{\boldsymbol{x}}_k$. All future EKF processing after a missed outlier should be suspect, but it is not, as the situation is undetected. $\triangle$

Remark 3. For the EKF, once the residual $\delta\boldsymbol{z}_k$ is computed, the measurements $\tilde{\boldsymbol{z}}_k$ are discarded. This is because, assuming that all outlier decisions are correct, the Markov modeling assumptions underlying the derivation of eqn. (9) render these measurements redundant. They have no further utility. However, if the outlier decisions could later be reconsidered, those measurements could have great utility in reconstructing the state trajectory between the time of the incorrect decisions and the present time. $\triangle$

3.2 Iterated Extended Kalman Filter (IEKF)

Assuming that the *a posteriori* IEKF solution (Maybeck (1979); Jazwinski (1970)) at t_{k-1} provided $\hat{\boldsymbol{x}}_{k-1}$ and $\boldsymbol{P}_{k-1}$ such that $\boldsymbol{x}_{k-1} \sim N(\hat{\boldsymbol{x}}_{k-1}, \boldsymbol{P}_{k-1})$, the IEKF aiding measurement update at time k solves

$$\hat{\boldsymbol{x}}_k = \arg\max_{\boldsymbol{x}_k, \boldsymbol{x}_{k-1}} \Big(p_{\boldsymbol{x}_{k-1}}\big(\boldsymbol{x}_{k-1} - \hat{\boldsymbol{x}}_{k-1}\big) \tag{11}$$

$$p_{\boldsymbol{\omega}_k}\big(\boldsymbol{x}_k - \boldsymbol{\phi}(\boldsymbol{x}_{k-1}, \mathbf{U}_{k-1})\big)p_{\boldsymbol{\eta}_k}\big(\tilde{\boldsymbol{z}}_k - \boldsymbol{h}(\boldsymbol{x}_k)\big)\Big),$$

Dropping the $\mathbf{U}_{k-1}$ from $\boldsymbol{\phi}(\boldsymbol{x}_{k-1}, \mathbf{U}_{k-1})$, the log-likelihood function is

$$L(\boldsymbol{x}_k, \boldsymbol{x}_{k-1}) = (\tilde{\boldsymbol{z}}_k - \boldsymbol{h}(\boldsymbol{x}_k))^\top \boldsymbol{R}_k^{-1} (\tilde{\boldsymbol{z}}_k - \boldsymbol{h}(\boldsymbol{x}_k)) \tag{12}$$

$$+ (\boldsymbol{x}_k - \boldsymbol{\phi}(\boldsymbol{x}_{k-1}))^\top \mathbf{Q}_{k-1}^{-1} (\boldsymbol{x}_k - \boldsymbol{\phi}(\boldsymbol{x}_{k-1}))$$

$$+ (\boldsymbol{x}_{k-1} - \hat{\boldsymbol{x}}_{k-1})^\top \boldsymbol{P}_{k-1}^{-1} (\boldsymbol{x}_{k-1} - \hat{\boldsymbol{x}}_{k-1}),$$

yielding a nonlinear least squares problem to be solved at each measurement time instant. This can be solved by various iterative methods. Let $t_k^* \in (t_k, t_{k+1})$ denote the time at which this nonlinear optimization process concludes.

Throughout the time interval $t \in [t_k, t_k^*]$ required to complete the nonlinear optimization, the INS keeps integrating the state estimate that it had started at t_{k-1}^* based on $\hat{\boldsymbol{x}}_{k-1}$ which became available at t_{k-1}^*. Once $\hat{\boldsymbol{x}}_k$ becomes available at t_k^*, the INS starts from that state and continues integrating. Therefore, the INS always maintains a real-time state estimate. This estimate does have discontinuous changes in value following measurement updates, just as the KF and EKF do.

This formulation allows the IEKF to adjust both $\boldsymbol{x}_k$ and $\boldsymbol{x}_{k-1}$. At the conclusion of the iterative process, optimal estimates for the state at both time instants are available however, only $\hat{\boldsymbol{x}}_k$ and its covariance $\boldsymbol{P}_k$ are retained. The improved estimate of $\boldsymbol{x}_{k-1}$, which is a smoothed estimate, is old relative to real-time and is simply discarded.

The IEKF can yield improved performance relative to the EKF in situations where the uncertainty in the prior state is significant relative to the higher order terms in the Taylor series representations of the nonlinearities $\boldsymbol{h}$ or $\boldsymbol{\phi}$.

Remark 4. In the IEKF, $\hat{\boldsymbol{x}}_{k-1}$ and the covariance $\boldsymbol{P}_{k-1}$ are unchangeable and assumed to be without error. The issues related to false detections and missed outliers as stated in Remarks 2 and 3 still apply. $\triangle$
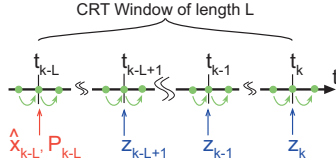
Fig. 1. Timeline for a CRT window with L aiding measurements.

3.3 Contemplative Real-time Estimator (CRT)

The CRT approach retains the prior at the start, and all aiding and IMU measurement data over the *CRT time window* $(t_{k-L}, t_k]$, where the CRT window length L is a positive integer (Ramanandan et al. (2011); Chen et al. (2013)). This set of data includes:

- the prior distribution for the state:

$$\boldsymbol{x}(t_{k-L}) \sim N(\hat{\boldsymbol{x}}_{k-L}, \boldsymbol{P}_{k-L});$$

- IMU measurements: $\mathbf{U} = \cup_{j=k-L}^{k-1} \mathbf{U}_j$; and
- Aiding measurements: $\mathbf{Z} = \{\tilde{\boldsymbol{z}}_j\}_{j=k-L+1}^{k}$.

The CRT objective is to estimate the optimal state trajectory $\mathbf{X}_k = \{\boldsymbol{x}(t_j)\}_{j=k-L}^{k}$ based upon sensor measurements $\mathbf{U}$ and $\mathbf{Z}$, and the prior density $p_{\boldsymbol{x}_{k-L}}(\boldsymbol{x}(t_{k-L}))$. This CRT approach is closely related to the methods used in the SLAM literature (Dellaert and Kaess (2006); Eustice et al. (2006); Kuemmerle et al. (2011); Li and Mourikis (2013)). The cost function that results is closely related to those in the moving horizon estimation approach (Tenny and Rawlings (2001); Haseltine and Rawlings (2005)).

Fig. 1 depicts a typical CRT window. The green dots on the time-line indicate IMU measurement times τ_i. The state transition between these times (indicated as green arcs) is constrained by the kinematic model of eqn. (2) and the IMU data $\mathbf{U}$. Additional constraints are imposed by the initial state estimate (i.e., $\hat{\boldsymbol{x}}(t_{k-L}), \boldsymbol{P}(t_{k-L})$) and aiding measurements $\mathbf{Z}$ shown below the time-line. Each of these constraints is quantified by a probability density that enables the Bayesian problem formulation. While Fig. 1 depicts all aiding measurements occurring at the IMU measurement time, unaligned measurements can be addressed by interpolation, and unknown latencies can be calibrated (Li and Mourikis (2014)).

Given standard assumptions concerning the model being Markov and the noise sources being mutually independent and white, the joint density $p(\mathbf{X}_k, \mathbf{U}, \mathbf{Z})$ simplifies to

$$p(\mathbf{X}_k, \mathbf{U}, \mathbf{Z}) = p_{\boldsymbol{x}_{k-L}}(\boldsymbol{x}_{k-L}) \prod_{j=k-L+1}^{k} p_{\boldsymbol{\eta}_k}(\boldsymbol{z}_j | \boldsymbol{x}_j)$$
$$\prod_{j=k-L+1}^{k} p_{\boldsymbol{\omega}_k}(\boldsymbol{x}_j | \boldsymbol{x}_{j-1}, \mathbf{U}_{j-1}).$$

The corresponding log-likelihood function $L(\boldsymbol{X}_k)$ is

$$\sum_{j=k-L+1}^{k} (\tilde{\boldsymbol{z}}_j - \boldsymbol{h}(\boldsymbol{x}_j))^\top \boldsymbol{R}_j^{-1} (\tilde{\boldsymbol{z}}_j - \boldsymbol{h}(\boldsymbol{x}_j)) \qquad (13)$$
$$+ \sum_{j=k-L+1}^{k} (\boldsymbol{x}_j - \boldsymbol{\phi}(\boldsymbol{x}_{j-1}))^\top \mathbf{Q}_{j-1}^{-1} (\boldsymbol{x}_j - \boldsymbol{\phi}(\boldsymbol{x}_{j-1}))$$
$$+ (\boldsymbol{x}_{k-L} - \hat{\boldsymbol{x}}_{k-L})^\top \boldsymbol{P}_{k-L}^{-1} (\boldsymbol{x}_{k-L} - \hat{\boldsymbol{x}}_{k-L}),$$

yielding a nonlinear least squares problem to be solved iteratively at each measurement time instant. As discussed relative to the IEKF, the CRT approach maintains a real-time state estimate at all times. The CRT and IEKF approaches are closely related, with the same results when $L = 1$.

Remark 5. The standard EKF assumptions in Remark 1 ensure $\boldsymbol{P}_{k-L}$ and $\mathbf{Q}_{j-1}$ for $j = k-L+1, \ldots, k$ are positive definite; therefore, the linearized solution at each iteration is well-defined. Having all the IMU and aiding measurements available across the CRT window, the approach is able to make and reconsider outlier decisions throughout that window. $\triangle$

4. CRT IMPLEMENTATION

Research reported in the SLAM and field robotics literature present efficient approaches to solve likelihood functions such as eqn. (13), even when L and m are large.

The algorithm will involve the following processes.

(1) Given a trajectory estimate at iteration l,
$$\hat{\mathbf{X}}_k^l = \{\hat{\boldsymbol{x}}_j^l \text{ for } j = k - L, \ldots, k\},$$
which is treated as a vector in $\mathbb{R}^{n(L+1)}$, an optimization algorithm computes a correction $\delta\boldsymbol{X}^l \in \mathbb{R}^{n(L+1)}$ such that
$$\hat{\mathbf{X}}^{l+1} = \hat{\mathbf{X}}^l + \delta\boldsymbol{X}^l \qquad (14)$$
is an improved solution to the optimization problem.
(2) Evaluation of each measurement in $\mathbf{Z}$ to detect and accommodate outliers.

Various alternative implementations are possible. The following describes the implementation used in Section 5.

4.1 Initialization of iteration at t_k

For the CRT measurement scenario depicted in Fig. 1. Minimization of eqn. (13) at the last measurement time t_{k-1} provided $\bar{\mathbf{X}}_{k-1} = \{\bar{\boldsymbol{x}}(t_j)\}_{j=k-L-1}^{k-1}$. In addition, $\boldsymbol{P}_{k-L}$ and $\boldsymbol{P}_{k-1}$ can be computed using the approach of eqns. (14-17) in (Kaess et al. (2008)). The error covariance $\boldsymbol{P}_{k-L}$ will be needed at t_k to compute the third term of eqn. (13). The error covariance $\boldsymbol{P}_{k-1}$ can be propagated to $\boldsymbol{P}_k^-$ using eqn. (8) which is useful for judging the measurement validity of $\boldsymbol{z}(t_k)$, when they arrive, before starting the optimization iterations at t_k.

INS integration in real-time starting from $\bar{\boldsymbol{x}}(t_{k-1})$ over the interval $[t_{k-1}, t_k]$ provides $\bar{\boldsymbol{x}}(t_k)$. Therefore, when the CRT optimization process starts when $t = t_k$, an initial trajectory for the iterative optimization can be defined as $\hat{\mathbf{X}}_k^0 = \{\bar{\boldsymbol{x}}(t_j)\}_{j=k-L}^{k}$ over the CRT window. Vector $\bar{\boldsymbol{x}}(t_{k-L-1})$ from $\bar{\mathbf{X}}_{k-1}$ is discarded.

4.2 Preoptimization outlier detection

At time k, the aiding measurement $\boldsymbol{z}_k$ and INS state estimate $\hat{\boldsymbol{x}}_k = \bar{\boldsymbol{x}}(t_k)$ are available; therefore, the residual measurement $\delta\boldsymbol{z}_k$ can be computed. The null hypothesis is that $\delta\boldsymbol{z}_k \sim N(\boldsymbol{0}, \boldsymbol{S}_k)$, where $\boldsymbol{S}_k = \boldsymbol{H}_k \boldsymbol{P}_k^- \boldsymbol{H}_k^\top + \boldsymbol{R}_k$. This hypothesis can be evaluate using standard statistical hypothesis testing methods (Baarda (1968); Hewitson et al. (2004)) to remove obvious outliers before they affect the optimization process.

4.3 Optimization

For the IEKF and CRT approaches, eqns. (12) and (13) have the form $\|\mathbf{v}(\mathbf{X})\|_\mathbf{W}^2 = \mathbf{v}(\mathbf{X})^\top \mathbf{W}^{-1} \mathbf{v}(\mathbf{X})$. The vector $\mathbf{v}(\mathbf{X})$ is the concatenation of each of the vectors summed in the log-likelihood function. The matrix $\mathbf{W}$ is block diagonal and positive definite, formed by the positive definite submatrices $\mathbf{R}_j$, $\mathbf{P}_{k-L}$ and $\mathbf{Q}_{j-1}$ for $j = k - L + 1, \ldots, k$.

Note that $\|\mathbf{v}\|_\mathbf{W} = \|\boldsymbol{r}\|_2$ where $\boldsymbol{r} \triangleq \boldsymbol{\Sigma}_W \mathbf{v}$ and $\mathbf{W}^{-1} = \boldsymbol{\Sigma}_W^\top \boldsymbol{\Sigma}_W$. In particular,

$$\boldsymbol{r}(\boldsymbol{X}) = \begin{bmatrix} \boldsymbol{\Sigma}_{\mathbf{P}_{k-L}} \left(\boldsymbol{x}_{k-L} - \hat{\boldsymbol{x}}_{k-L}\right) \\ \boldsymbol{\Sigma}_{\mathbf{Q}_{k-L}} \left(\boldsymbol{\phi}(\boldsymbol{x}_{k-L}, \mathbf{U}_{k-L}) - \boldsymbol{x}_{k-L+1}\right) \\ \vdots \\ \boldsymbol{\Sigma}_{\mathbf{Q}_{k-1}} \left(\boldsymbol{\phi}(\boldsymbol{x}_{k-1}, \mathbf{U}_{k-1}) - \boldsymbol{x}_k\right) \\ \boldsymbol{\Sigma}_{\mathbf{R}_{k-L+1}} \left(\boldsymbol{h}(\boldsymbol{x}_{k-L+1}) - \tilde{\boldsymbol{x}}_{k-L+1}\right) \\ \vdots \\ \boldsymbol{\Sigma}_{\mathbf{R}_k} \left(\boldsymbol{h}(\boldsymbol{x}_k) - \tilde{\boldsymbol{z}}_k\right) \end{bmatrix}.$$

With this notation, each log-likelihood minimization problem reduces to a nonlinear least square optimization

$$\min_{\mathbf{X} \in \mathbb{R}^{n(L+1)}} \|\boldsymbol{r}(\mathbf{X})\|_2^2. \qquad (15)$$

Let $\mathbf{J}$ represent the Jacobian matrix of $\boldsymbol{r}(\mathbf{X})$ with respect to $\mathbf{X}$ evaluated at $\hat{\mathbf{X}}$. This Jacobian is sparse. The vector $\boldsymbol{\delta X}$ is the solution of

$$\mathbf{J}\delta\boldsymbol{X} = \boldsymbol{r}, \qquad (16)$$

which can be solved efficiently for $\delta\boldsymbol{X}$ by Cholesky factorization (Dellaert and Kaess (2006)) or Givens rotations (Kaess et al. (2008)).

4.4 Outlier Detection during optimization

After the iteration converges, the residual vector $\boldsymbol{r}$ is expected to be zero mean with unit variance. Each residual is compared against a decision threshold to either accept or reject the measurement. This is performed for all aiding sensor residuals, but not for the INS or prior residuals, which are assumed to be error free. If any aiding sensor residuals are rejected, then the optimization is performed again, followed by the residual check, until the optimization completes and no additional measurements are rejected.

5. EXPERIMENTAL RESULTS

This section compares the EKF, IEKF, and CRT (with window length L) estimators. All algorithms are implemented using exactly the same IMU and single frequency

(L1) Global Positioning System (GPS) data in post-processing, to enable direct comparison. Even though this comparison is achieved in post-processing, each algorithm is written in C++ to run in a real-time (Linux RT kernel).

Because the data is available for post-processing, we are also able to implement (as a batch process) a MAP estimator for the entire trajectory using all the data, including two-frequency GPS integer-resolved carrier phase (Vu et al. (2013)). The output of this batch smoother is declared as the "ground truth" trajectory and has accuracy at the centimeter level.

The trajectory is frequently under trees and adjacent to tall buildings, creating numerous outlier GPS measurements. Note that this example implementation must accommodate the reality that the number of measurements m is time-varying, as discussed in the last paragraph of Section 2.2.

While the vehicle is driven, the sensor data is time-stamped and stored. The sensor data includes 200Hz MEMS IMU data (NAVCN NV-IMU1000) and 1Hz L1/L2 Differential GPS data (NovAtel OEMV-3). For all the real-time algorithm results to be discussed below, position is initialized from GPS before the algorithm begins; roll and
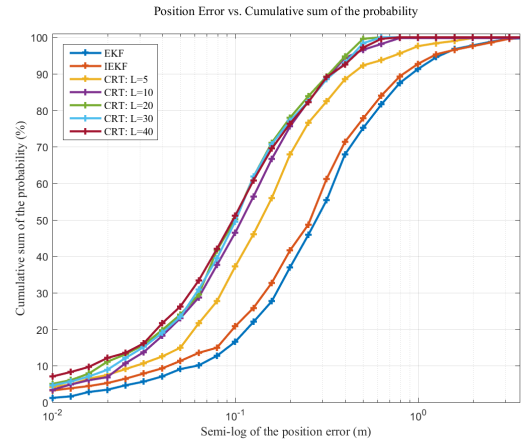

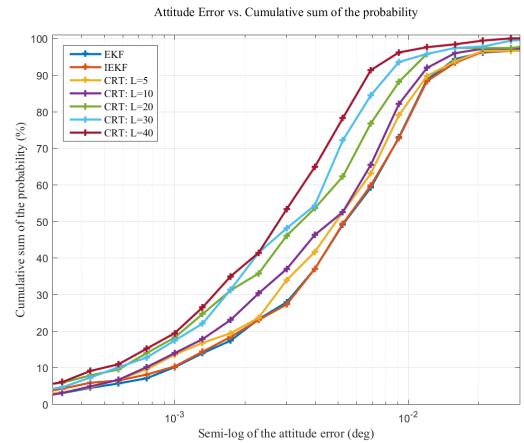Fig. 2. Cumulative distribution of position error for each algorithm.

Fig. 3. Cumulative distribution of attitude error for each algorithm.

pitch are initialized from IMU data by standard methods; velocity, yaw, and bias estimates are all initialized to zero.

The results of the real-time algorithms are compared to the ground truth trajectory to enable quantifiable comparisons of results between estimation approaches. For example, the position error for algorithm $\star$ would be $\|\hat{p}_\star(t_k) - \hat{p}_g(t_k)\|$ where 'g' is the ground truth position and $\star$ can be EKF, IEKF, or CRT (of length L). The trajectory is 495 seconds long, yielding the same number of error samples per algorithm. The position and attitude error cumulative distribution functions (CDFs) of each algorithm are shown in Figs. 2 and 3. The figures indicate that accuracy improves from the EKF to the IEKF to the CRT. Also, CRT performance (generally) increases with the window length L. The CRT algorithms with $L > 20$ each achieve $0.6m$ accuracy on 100% of the trajectory. Similarly, the EKF and IEKF CDF plots do not reach 100% until the accuracy is over $3.0m$.

6. DISCUSSION

The EKF, IEKF, and CRT approaches are very closely related. Each cost function can be represented in the form of a normalized residual vector as in eqn. (15). For the EKF, the argument would be $\delta\mathbf{X}$ instead of $\mathbf{X}$.

The EKF at each time step has n variables to estimate (one state vector) and $m = n + m$ constraints (GPS and prior); therefore, the degrees of freedom (DOF) is m. For the IEKF, the number of variables to be estimated is $2n$ and the number of constraints is $m + 2n$; therefore, the DOF is still m. The main advantage of the IEKF over the EKF is its ability to perform a nonlinear iterative correction.

For the CRT algorithm with window length L, the number of variables to be estimated is $(L+1)n$. The number of constraints is $(L+1)n + Lm$. The DOF is therefore, Lm.

Both the outlier detection capability and the amount of required computation increase with L. For $L = 1$ the IEKF and CRT approaches are the same. For $L > 1$ the CRT is able to outperform the IEKF because the larger DOF allows the CRT to more effectively remove the effects of outlier measurements as long as they are within the CRT window. Because there are far more measurements within the window than are necessary for state observability (see Remark 5) measurement rejection can be aggressive. The goal of outlier rejection is to ensure that all measurements used in the computation of $\hat{x}_{k-L}$ and $\boldsymbol{P}_{k-L}$ be ensured to be valid.

7. CONCLUSIONS

Often to achieve higher accuracy or better reliability for autonomous vehicle state estimation the first impulse is to consider upgrading the sensor suite. This article has taken the opposite approach, looking at alternative algorithms for state estimation, using exactly the same sensor data, and demonstrating that significant (i.e., tenfold) performance enhancements are possible. This motivates the idea that investments in improved algorithms, and the computers to implement them, could yield as significant performance enhancements as investments in better sensors.

Additional research is required on computationally efficient methods to effectively accommodate outlier measurements.

REFERENCES

Baarda, W. (1968). A Testing Procedure for Use in Geodetic Networks. *Netherlands Geod. Comm.*, 2(4).

Brown, R.G. and Hwang, P.Y. (1983). A Kalman filter approach to precision GPS geodesy. *Navigation*, 30(4), 338–349.

Chen, Y., Zheng, D., Miller, P.M., and Farrell, J. (2013). Underwater Vehicle Near Real Time State Estimation. In *Proc. IEEE MSC*.

Dellaert, F. and Kaess, M. (2006). Square Root SAM: Simultaneous Localization and Mapping via Square Root Information Smoothing. *Int. J. Rob. Res.*, 25(12), 1181–1203.

Eustice, R.M., Singh, H., and Leonard, J.J. (2006). Exactly Sparse Delayed-State Filters for View-Based SLAM. *IEEE T. Rob.*, 22(6), 1100–1114.

Farrell, J., Givargis, T., and Barth, M. (2000). Real-time Differential Carrier Phase GPS-aided INS. *IEEE Trans. CST*, 8(4), 709–721.

Farrell, J.A. (2008). *Aided Navigation: GPS with High Rate Sensors.* McGraw Hill.

Haseltine, E. and Rawlings, J. (2005). Critical evaluation of extended kalman filtering and moving-horizon estimation. *Ind. Eng. Chem. Res.*, 44, 2451–2460.

Hewitson, S., Lee, H.K., and Wang, J. (2004). Localizability Analysis for GPS/Galileo Receiver Autonomous Integrity Monitoring. *J. of Navigation*, 57, 245–259.

Jazwinski, A.H. (1970). *Stochastic Processes and Filtering.* Mathematics in Science and Engineering. Academic Press.

Kaess, M., Ranganathan, A., and Dellaert, F. (2008). iSAM: Incremental Smoothing and Mapping. *IEEE T. Rob.*, 24(6), 1365–1378.

Kalman, R. (1960). A new approach to linear filtering and prediction problems. *J. of Bas. Eng.*, 35–45.

Kalman, R. and Bucy, R. (1961). New results in linear filtering and prediction theory. *J. of Bas. Eng.*, 95–108.

Kuemmerle, R., Grisetti, G., Strasdat, H., Konolige, K., and Burgard, W. (2011). g2o: A general framework for graph optimization. In *ICRA*.

Li, M. and Mourikis, A.I. (2013). High-precision, consistent EKF-based visual–inertial odometry. *Int. J. of Rob. Res.*, 32(6), 690–711.

Li, M. and Mourikis, A.I. (2014). Online temporal calibration for camera–IMU systems: Theory and algorithms. *Int. J. of Rob. Res.*, 33(7), 947–964.

Maybeck, P.S. (1979). *Stochastic Models, Estimation, and Control.* Mathematics in Science and Engineering. Academic Press.

Ramanandan, A., Chen, A., and Farrell, J. (2011). A Near-Real Time Nonlinear State Estimation Approach with Application to Initialization of Navigation Systems. In *IEEE CDC*.

Tenny, M.J. and Rawlings, J.B. (2001). State estimation strategies for nonlinear model predictive control. In *AIChE Annual Meeting*.

Vu, A., Farrell, J.A., and Barth, M. (2013). Centimeter-accuracy smoothed vehicle trajectory estimation. *IEEE Intell. Transp. Syst. Mag.*, 5(4), 121–135.